Molecular Cancer

RESEARCH

Open Access

# Proapoptotic activity of JNK-sensitive BH3-only proteins underpins ovarian cancer response to replication checkpoint inhibitors

Annapoorna Venkatachalam[1,2], Cristina Correia[2], Kevin L. Peterson[2], Xianon Hou[2], Paula A. Schneider[2], Annabella R. Strathman[2], Karen S. Flatten[2], Chance C. Sine[2], Emily A. Balczewski[2,3], Cordelia D. McGehee[1], Melissa C. Larson[4], Laura N. Duffield[2], X. Wei Meng[2], Nicole D. Vincelette[1,5], Husheng Ding[2], Ann L. Oberg[6], Fergus J. Couch[7], Elizabeth M. Swisher[8], Hu Li[1], S. John Weroha[1,2] and Scott H. Kaufmann[1,2,9*]

## Abstract

Recent studies indicate that replication checkpoint modulators (RCMs) such as inhibitors of CHK1, ATR, and WEE1 have promising monotherapy activity in solid tumors, including platinum-resistant high grade serous ovarian cancer (HGSOC). However, clinical response rates are generally below 30%. While RCM-induced DNA damage has been extensively examined in preclinical and clinical studies, the link between replication checkpoint interruption and tumor shrinkage remains incompletely understood. Here we utilized HGSOC cell lines and patient-derived xenografts (PDXs) to study events leading from RCM treatment to ovarian cancer cell death. These studies show that RCMs increase CDC25A levels and CDK2 signaling in vitro, leading to dysregulated cell cycle progression and increased replication stress in HGSOC cell lines independent of homologous recombination status. These events lead to sequential activation of JNK and multiple BH3-only proteins, including BCL2L11/BIM, BBC3/PUMA and the BMF, all of which are required to fully initiate RCM-induced apoptosis. Activation of the same signaling pathway occurs in HGSOC PDXs that are resistant to poly(ADP-ribose) polymerase inhibitors but respond to RCMs ex vivo with a decrease in cell number in 3-dimensional culture and in vivo with xenograft shrinkage or a significantly diminished growth rate. These findings identify key cell death-initiating events that link replication checkpoint inhibition to antitumor response in ovarian cancer.

**Keywords** High grade serous ovarian cancer, Apoptosis, CHK1 inhibitor, ATR inhibitor, WEE1 inhibitor, BH3 proteins, Replication stress

*Correspondence:
Scott H. Kaufmann
Kaufmann.Scott@Mayo.edu
[1] Department of Molecular Pharmacology & Experimental Therapeutics, Mayo Clinic, 200 First Street, S.W., Rochester, MN 55905, USA
[2] Department of Oncology, Mayo Clinic, 200 First Street, S.W., Rochester, MN 55905, USA
[3] Present Address: Department of Computational Medicine and Bioinformatics, University of Michigan Medical School, Ann Arbor, MI 48109, USA
[4] Division of Clinical Trials and Biostatistics, Mayo Clinic, 200 First Street, S.W., Rochester, MN 55905, USA
[5] Present Address: H. Lee Moffitt Cancer Center, Tampa, FL 33612, USA
[6] Division of Computational Biology, Department of Quantitative Health Sciences, Mayo Clinic, 200 First Street, S.W., Rochester, MN 55905, USA
[7] Division of Experimental Pathology, Department of Laboratory Medicine, and Pathology, Mayo Clinic, 200 First Street, S.W., Rochester, MN 55905, USA
[8] Department of Obstetrics and Gynecology, University of Washington, 1959 NE Pacific Street, Seattle, WA 98195, USA
[9] Division of Hematology, Department of Medicine, Mayo Clinic, 200 First Street, S.W., Rochester, MN 55905, USA

## Introduction

Ovarian, fallopian tube, and primary peritoneal cancers (termed "ovarian cancer" herein) constitute a heterogeneous group of neoplasms that annually affect 22,000 patients in the U.S. and have the highest mortality of any gynecological cancer [1]. Among these neoplasms, high-grade serous ovarian cancer (HGSOC) is the most lethal [2], accounting for over 200,000 cancer deaths per year worldwide [3]. Approximately 50% of HGSOCs are homologous recombination (HR) deficient (HRD) due to silencing or inactivation of HR repair genes [4]. Importantly, the HRD subset shows a better response to platinum-based chemotherapy. Moreover, addition of PARP inhibitor (PARPi) therapy has extended the duration of progression-free survival in HGSOC, particularly in cases with *BRCA1* or *BRCA2* mutations, reflecting the synthetic lethality of *BRCA1/2* loss and PARP1 inhibition [5–7]. Nonetheless, even within this subset that derives the most benefit from PARPi therapy the majority of ovarian cancer patients relapse and die of their disease [8], highlighting the need for improved treatment.

Comprehensive characterization of ovarian cancers has shown that replication stress (RS), like HR deficiency, is widespread in HGSOC, creating another important vulnerability, albeit one that is not directly actionable [9, 10]. Moreover, a variety of studies have shown that treatment with inhibitors of replication checkpoint kinases, including ATR, CHK1, and WEE1, increase this RS, enhancing the effects of chemotherapies that induce replication stress or leading to cell death on their own [11, 12]. Consistent with these preclinical studies, promising clinical activity of combinations containing the current generation of replication checkpoint modulators (RCMs) has been observed in advanced solid tumors, including ovarian cancer [13–16]. Moreover, evidence of single agent activity has also been observed [17, 18]. Importantly, phase II trials of the CHK1i prexasertib in platinum-resistant or -refractory HGSOC demonstrated responses in cases that recurred after prior PARPi, suggesting that prexasertib might be beneficial in PARPi resistant disease [12, 18, 19]. Additionally, the WEE1i adavosertib has also been reported to have substantial activity in PARPi-resistant ovarian cancer, particularly in combination with olaparib (ClinicalTrials.gov identifier NCT03579316).

Because the efficacy of ATR, CHK1, and WEE1 inhibitor monotherapy in advanced ovarian cancer is modest, ranging from 6–30% in various studies [18, 20, 21], the identification of biomarkers that would allow selection of patients most likely to respond to RCMs would be beneficial. To this end, a variety of potential biomarkers of RCM sensitivity have been proposed, including HR deficiency, ATM inactivation, *CCNE1* and/or *MYC* amplification, and biochemical evidence of RS as manifested by phosphorylation of CHK1, H2AX or RPA32 [12, 13, 22].

While previous efforts to identify predictive biomarkers for RCM response have focused on events proximate to replication fork disturbance, a large number of steps undoubtedly occur between enhancement of RS by RCMs and cancer cell death. Relatively little is known about these intervening steps. Although a recent study in acute monocytic leukemia cells indicated that RCMs kill through a pathway involving activation of the stress kinase JNK leading to JUN/FOS-mediated *TNF* gene activation and subsequent TNFα-induced triggering of the extrinsic apoptotic pathway [23], TNF-mediated processes were able to account for only part of the leukemic cell death, suggesting that a second pathway might contribute. In addition, it also has been unclear whether the same extrinsic apoptotic pathway contributes to RCM activity in solid tumors.

Here we examined the association between previously identified biomarkers of RS and response of a series of HGSOC patient-derived xenografts (PDXs) to paradigmatic inhibitors of CHK1 (prexasertib), ATR (ceralasertib), and WEE1 (adavosertib) ex vivo and in vivo. Because models lacking these RS biomarkers also responded to the RCMs, we additionally performed an in-depth analysis of steps leading to RCM-induced HGSOC cell death that implicated the intrinsic apoptotic pathway and identified an important role for BMF, a BH3-only protein previously implicated in detachment-induced apoptosis [24, 25], in RCM-induced killing of solid tumor cells. Collectively, this analysis identified key signaling steps contributing to RCM-induced cell death that have the potential to modulate RCM sensitivity or resistance.

## Methods

### Materials

All reagents and antibodies are listed in Supplemental Table S1.

### Cell lines

Sources of cell lines are indicated in Supplemental Table S1. Cell lines were cultured in the following media: OVCAR8, OVCAR5, COV362, OV90, and IGROV1 cells in RPMI 1640 medium; CaOV3, PEO1, PEO1-derived PARP inhibitor resistant clones #2 and #3, and PEO4 cells in DMEM medium with high glucose supplemented with 10 µg/ml insulin, and 0.04 mM Dulbecco's nonessential amino acids; and SKOV3 cells in McCoy's 5A medium. Of these lines, SKOV3 has been classified as unlikely to be HGSOC based on genomic features and IGROV1 has been reported to be hypermutated [26]. All media contained 10% (vol/vol) heat-inactivated fetal bovine serum,

50 units/mL penicillin G, 50 µg/mL streptomycin, and 1 mM glutamine. All cell lines were authenticated by short tandem repeat profiling in the Mayo Clinic Cytogenetics Core Facility. In addition, PEO1 and PEO4 cells were confirmed to have their reported *BRCA2* mutations by Sanger sequencing [27]. Additionally, all cell lines were tested with the MycoAlert Mycoplasma Detection Kit (Lonza) and found to be mycoplasma-free.

To generate $FADD^{-/-}$ cells, oligonucleotides guiding to human *FADD* 228–237 (NM_003824.3) were synthesized, annealed, and cloned into the BsmBI site of lentiCRISPR-v2 plasmid (Addgene, Cambridge, MA). FADD targeting virus and empty vector (EV) were packaged by transfecting HEK293T cells with the packaging vector psPAX3, envelope vector pMD2.G, and lentiCRISPR-v2-FADD or EV using Lipofectamine 2000 (ThermoFisher, Waltham, MA). Two days after viral transduction, PE01 cells were selected with 3 µg/ml puromycin for a week, cloned by limiting dilution in 96-well plates, and assayed for gene interruption by immunoblotting. A similar process was used to generate $BID^{-/-}$ cells and $BAX^{-/-}/BAK^{-/-}$ (DKO) cells using oligos that target human *BID* 591–610 (NM_197966.2), human *BAK* 162–184 (AF520590.1), and human *BAX* 179–201 (NM_001291428.1).

For transient transfections, aliquots containing ~ $1 \times 10^7$ cells were transfected with 40 µM siRNA and subjected to electroporation using a BTX830 square wave electroporator (BTX, San Diego, CA) delivering two 10-ms pulses at 280 V and harvested for immunoblotting or assayed for drug sensitivity as indicated in the individual figure legends.

#### Colony forming assays

For clonogenic assays, cells were plated for 12–16 h before drugs were added and monitored continuously for 10–14 days until colonies of ~ 50 cells formed in control wells. Plates were then stained with Coomassie blue so that visible colonies could be counted. Survival was calculated as the ratio of colonies treated with the drug compared with diluent.

#### RAD51 foci

Assays for irradiation-induced RAD51 foci were performed as previously described [28]. Cells plated on coverslips were irradiated (10 Gy) and incubated at 37 °C for 6 h before fixation in 4% (wt/vol) paraformaldehyde. Coverslips were incubated with primary antibody (1:500) in blocking buffer overnight at 4 °C. Coverslips were then washed 6 times with wash buffer (PBS containing 0.1% Triton X-100 and 0.1% bovine serum albumin), incubated with secondary antibody (Alexa fluor 488 goat anti-rabbit IgG and Alexa fluor 568 goat anti-mouse IgG, each at 1:1000) in blocking buffer for 1 h at 21 °C in the dark, washed, and counterstained with 1 µg/ml Hoechst 33258 in PBS. Samples were examined on a Zeiss Axiovert microscope with 63X/NA 1.4 lens and photographed using a Zeiss Axiocam MRm CCD camera using Zeiss Zen software. RAD51 foci were quantified manually in a blinded fashion in ≥ 100 cells per slide and considered positive if ≥ 10 Rad51 foci were visible.

#### Analysis of PDX generation and drug testing ex vivo

Patient-derived xenografts (PDXs) were generated in 6- to 7-week-old female SCID beige (C.B.17/IcrHsd-Prkdc$^{scid}$ Lyst$^{bg-J}$; Envigo RMS, LLC, Indianapolis IN) mice as previously described in detail [28, 29]. All procedures were conducted in accordance with Animal Welfare Regulations and were approved by the Institutional Animal Care and Use Committee (IACUC) at the Mayo Clinic (A37615).

Sensitivity of these PDXs to various agents ex vivo was assessed as described [30]. In brief, PDXs were harvested from mice, minced into 2- to 4-mm pieces, and dissociated using a gentleMACS cell dissociator (Miltenyi Biotech) following the supplier's protocol. Single-cell suspensions were then treated with the indicated drugs and plated in 24-well plates. Following 72 h or 5 days, cell viability was measured using CellTiter-Glo 3D (Promega). Cell viability was calculated for each concentration as an average of seven replicates and normalized to untreated vehicle controls.

#### Effects of WEE1i and ATRi in vivo

For all PDX studies, cryogenically preserved human ovarian cancer tumors were rapidly thawed and reestablished as previously described [29]. Four individual HGSOC models (PH061, PH063, PH0235 and PH354) were chosen based on previous PARP inhibitor response. Briefly, 0.1–0.2 cc of the minced tumor was prepared in 1:1 ratio with McCoy's 5A Modified Medium (Cat # MT-10–050-CV, Corning Life Science) before intraperitoneal injection. PDX engraftment was followed by abdominal palpation and transabdominal ultrasound using a SonoSite S-Series ultrasound machine (Fujifilm SoniSite, Inc). Tumor diameter was assessed using the on-board SonoSite software real-time measurement tool and cross-sectional area was measured on exported images using ImageJ software after calibration as described.

When intraperitoneal tumor area reached 0.5–1 $cm^2$, mice were randomized to treatment arms. Olaparib was given by daily oral gavage in 15% methylcellulose (50 mg/kg as monotherapy). Ceralasertib 35 mg/kg or adavosertib 80 mg/kg was administered 3 days/week by oral gavage. The largest tumor cross-sectional area was measured twice weekly through day 28. Mice were euthanized individually when moribund or as a cohort

at day 28. The primary endpoint was tumor area by ultrasound, normalized to the day 1 area of the same tumor and plotted as a ratio vs. time.

### Statistics and reproducibility

Dose–response curves were performed in cell lines at least three times independently. Error bars in all plots represent mean ± SEM of 3 independent experiments. *, ** and *** indicate $p < 0.05$, $p < 0.01$ and $p < 0.001$, respectively, using unpaired $t$ tests. Relative $IC_{50}$ values were analyzed in Microsoft® Excel by linear regression. Where indicated, analysis of variance (ANOVA, one-way or two-way as appropriate) with post-hoc correction for multiple comparisons was performed using GraphPad Prism 9 software. Immunoblots were performed in indicated cell lines at least two times independently.

### Additional methods

Methods for detection of apoptosis, cell fractionation, immunoblotting, qRT-PCR, RNAseq, and quantitative analysis of PDX growth ex vivo and in vivo have been previously published and are described in the Supplementary Methods.

## Results

### RCM monotherapy activity against PDXs ex vivo

To identify potential PDXs for in vivo testing, we first established short-term 3D cultures from 18 distinct PDXs with varied genomic backgrounds for testing ex vivo (Supplementary Table S2). These PDXs were all of the serous subtype, with 14 of the models established from primary tumor (Supplementary Table S3). Studies confirmed that PDX response to prexasertib was similar in snap frozen and fresh tissue (Supplementary Fig. S1A). Killing by prexasertib, ceralasertib, and adavosertib ex vivo varied across the models, with comparable median responses of 36% death with prexasertib, 34% with ceralasertib and 35% with adavosertib at 5 days (Fig. 1A-D), which is modest but would be considered a partial response in the clinical setting. Of the 18 PDXs, 10 had been previously assessed by clinical HRD tests. In these ovarian cancer PDXs treated ex vivo, response to RCM monotherapy did not correlate with HRD score (Fig. 1E).

In subsequent experiments, several molecular features of stressed replication forks were examined (Fig. 1F and G). RS at baseline as manifested by high γH2AX and phospho-Ser$^{4/8}$-RPA32 was observed in all PDXs and did not correlate with response ex vivo. There was, however, a trend toward lower CHK1 levels in models that

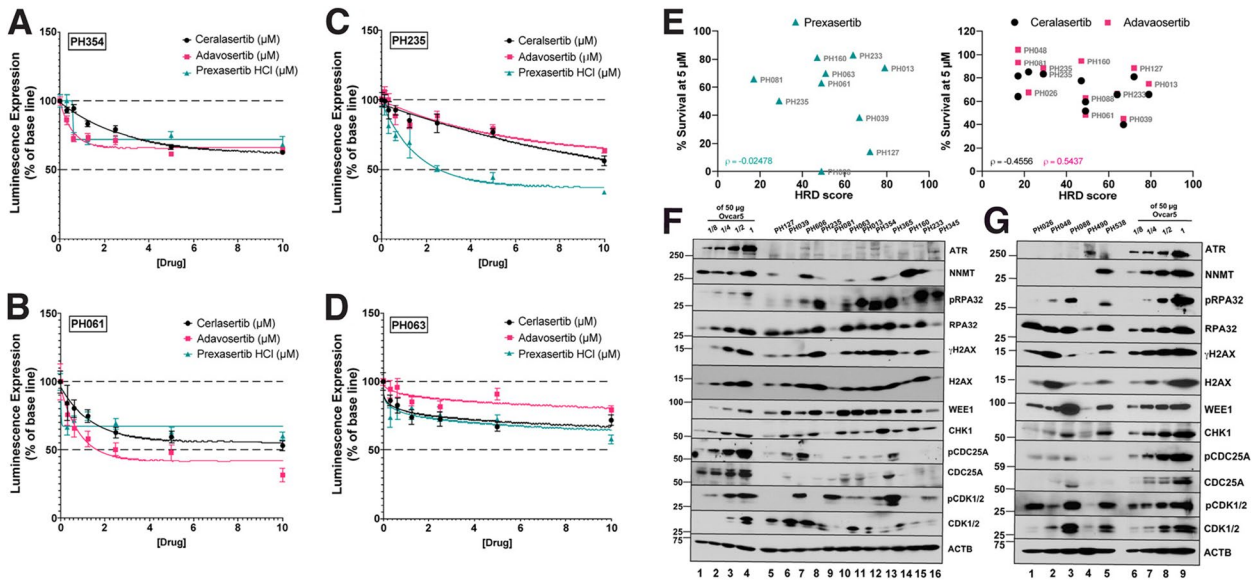


**Fig. 1** Analysis of RCM sensitivity in HGSOC PDXs ex vivo. **A-D**, Single-cell suspensions isolated from the indicated PDXs were plated and allowed to form 3D spheroids for 24 h. Cells were then treated with prexasertib, ceralasertib, or adavosertib for 72 h. Cell viability was assayed using RealTime-Glo™ MT Cell Viability Assay. Error bars, ± SEM of three independent experiments. **E**, Association between % survival at 5 μM prexasertib (left, $p = -0.02478$) or ceralasertib and adavosertib (right, $p = -0.4556$ and 0.5437, respectively) with HRD score using Spearman correlation. **F**, Indicated protein levels across ovarian carcinoma PDX [ordered by % survival at 5 μM to prexasertib (Table S2), with most sensitive toward the left] with serial dilutions of Ovcar5 cells. **G**, PDXs that were tested for sensitivity to ceralasertib and adavosertib but not prexasertib (ordered by % survival at 5 μM to ceralasertib, with most sensitive on the right)

were more sensitive to the CHK1i prexasertib, although this did reach statistical significance (Fig. S1B, $\rho = 0.566$, $p = 0.059$).

### WEE1i-induced tumor regressions independent of *CCNE* or *MYC* amplification

Focal amplifications involving the *CCNE1* and *MYC* loci, which are common in HGSOC, are harbingers of primary treatment failure and poor overall survival after standard-of-care platinum-based therapy [31, 32] but have been suggested to be associated with RCM sensitivity in previous studies [33–35]. To test this in vivo, four ovarian cancer PDX models that displayed moderate responses to CHK1, ATR, and WEE1 inhibitors ex vivo were treated with RCMs. All had *TP53* mutations and were known to be PARPi-resistant ($PARPi^{res}$), with three models wildtype for *BRCA1* and *BRCA2* and one having a *BRCA2* variant. Two of these PDXs (PH354 and PH235) were characterized as *CCNE* and *MYC* amplified (Table S2, highlighted in blue), with higher CCNE1 and MYC expression also detected by immunoblotting (Fig. S2A).

When mice bearing orthotopic xenografts were treated with diluent, the PARPi olaparib, the ATRi ceralasertib, or the WEE1i adavosertib over a 28-day period, treatment was well-tolerated, with no dose reductions required (Fig. S2B). Weekly transabdominal ultrasound indicated that none of the xenografts shrank below baseline in the olaparib arm (Fig. 2A-D), confirming that they are PARPi resistant by previously described response criteria [28].

Importantly, some of these PARPi-resistant PDXs responded to RCMs. In particular, adavosertib induced tumor shrinkage and prolonged survival in PH354

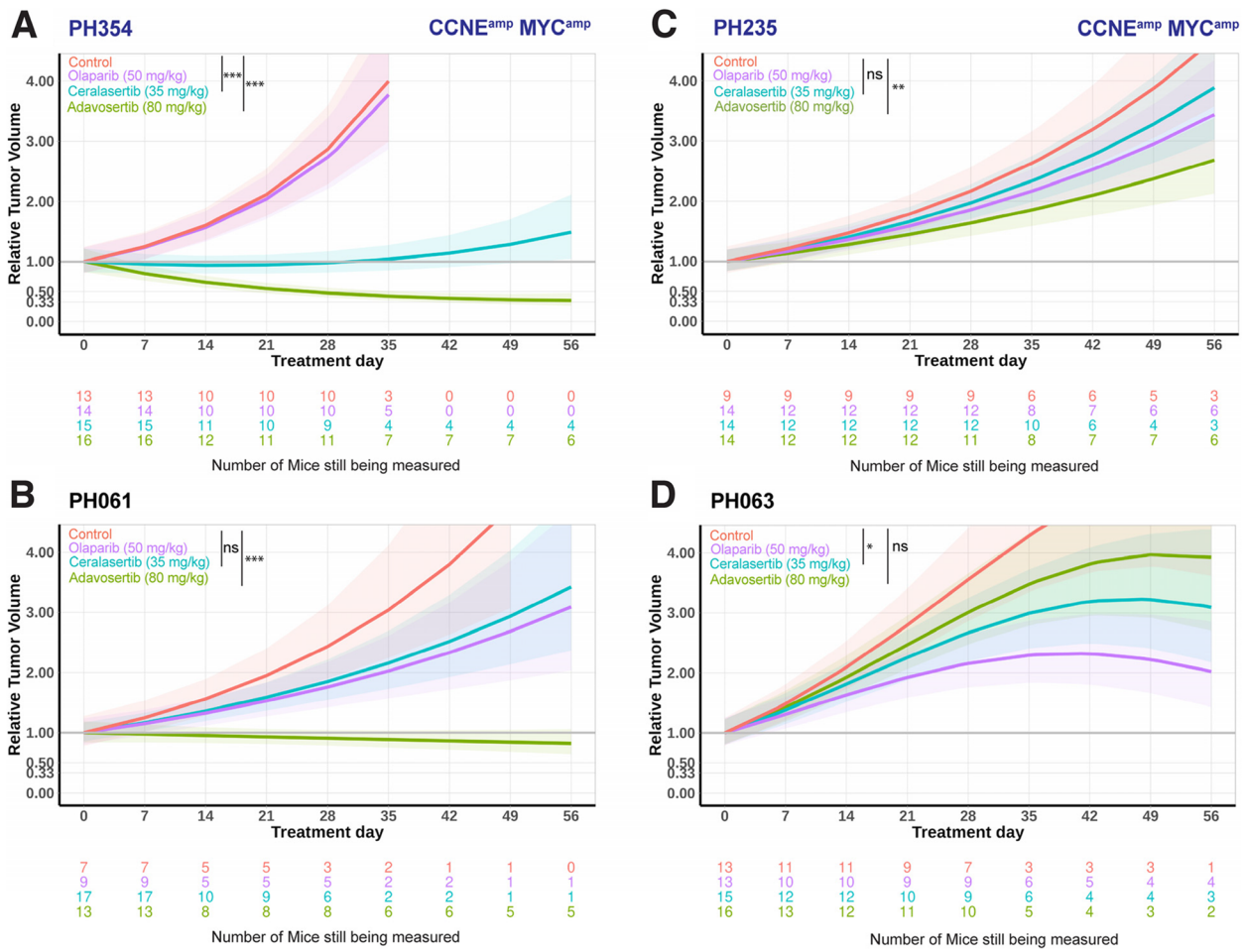


**Fig. 2** Response of HGSOC PDXs in vivo. Ceralasertib, adavosertib or olaparib were administered to mice bearing orthotopic HGSOC PDX models PH354 (A), PH235 (B), PH061 (C), or PH063 (D) with tumor growth measured by transabominal ultrasound. Following 4 weeks of treatment, tumor growth was observed for a minimum of 60 days unless the tumor met euthanasia criteria. The number of mice under observation is indicated below the *x*-axis, where text color indicates treatment arm. Shaded areas, 95% confidence intervals; pairwise comparisons for treatment arms are *, *** and ****: $p < 0.05$, $p < 0.001$, and $p < 0.0001$, respectively, for indicated global *p* value comparisons

(*CCNE*$^{amp}$ *MYC*$^{amp}$) and PH061 (diploid for *CCNE1* and *MYC*), with more extensive shrinkage in PH354 than in PH061 (Fig. 2A, B and S2C). In contrast, neither the *CCNE*$^{amp}$ *MYC*$^{amp}$ PDX PH235 nor the nonamplified PDX PH063 showed shrinkage below baseline during adavosertib treatment, although statistically significant growth inhibition was observed (Fig. 2C, D and S2C; Supplementary Table S4).

Overall, ceralasertib was less efficacious across all models at the dose administered. The best response, which was prolonged disease stabilization, was observed in the *CCNE*$^{amp}$ *MYC*$^{amp}$ PDX PH354, with some blunting of growth in PH063 (Fig. 2A and D) and little effect in *CCNE*$^{amp}$ *MYC*$^{amp}$ PH235 or nonamplified PH061 (Fig. 2B and C and Supplementary Table S4).

Because the lack of apparent association between RCM response and *CCNE* or *MYC* amplification differed from reported results in other preclinical studies, we also analyzed the association of HGSOC PDX sensitivity to prexasertib ex vivo (Fig. 1A-E) with expression of CCNE1 and MYC (Fig. S2D and E). As indicated in Fig. S2F, MYC levels were lower in sensitive PDXs. These results suggested that factors in addition to CCNE1 and/or MYC overexpression might be needed to predict HGSOC response to RCMs, prompting further investigation RCM-induced signaling.

### RCM sensitivity of ovarian cancer cell lines

As a starting point for these further studies, we assessed the clonogenic response of a panel of 11 ovarian cancer

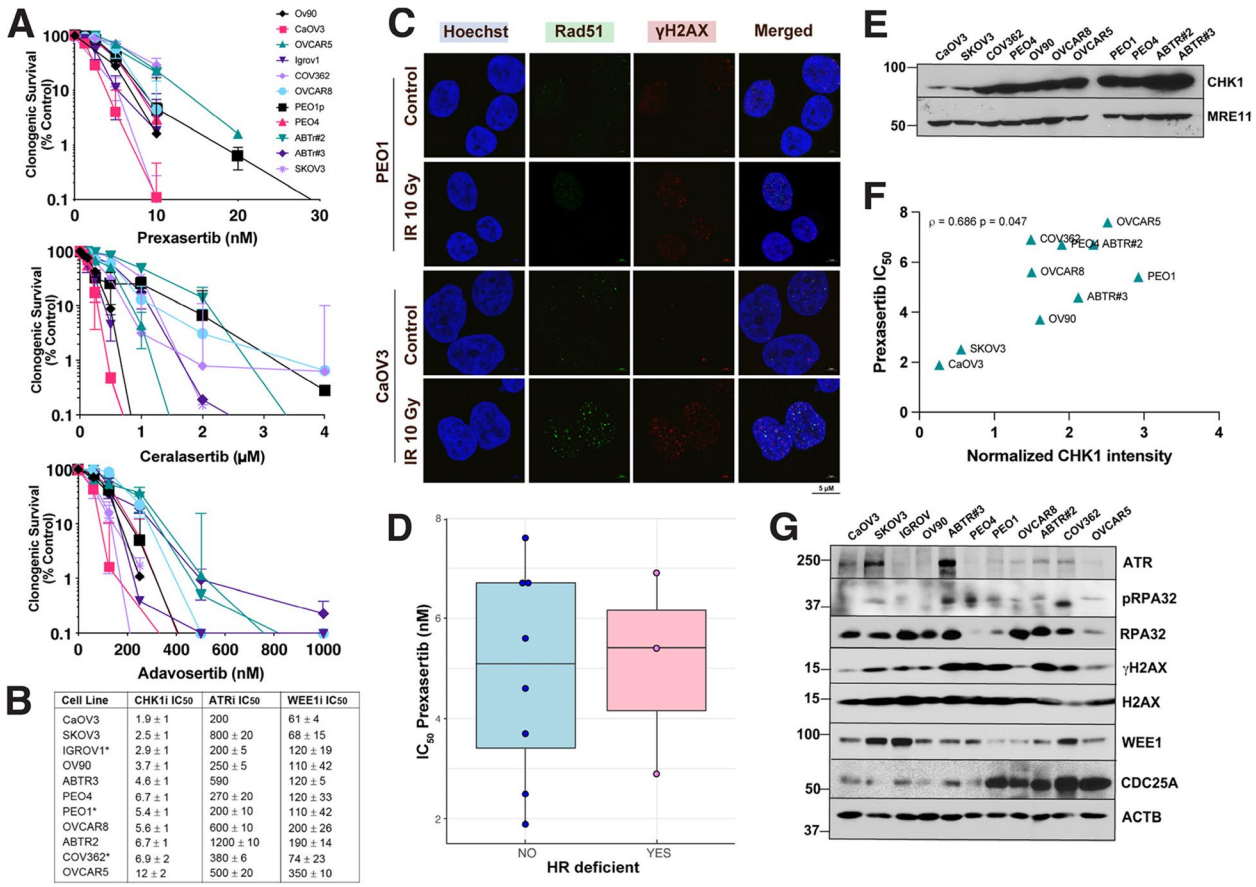


**Fig. 3** Effect of RCMs on HR deficient and HR proficient ovarian cancer cell lines. **A**, Cells were treated continuously with CHK1i (prexasertib), ATRi (ceralasertib) or WEE1i (adavosertib) in a clonogenic assay. Results are expressed as a percentage of colonies formed relative to cells treated with diluent alone. Error bars, ± SEM from three or more independent experiments. **B**, Relative $IC_{50}$s were estimated by linear regression from data in panel A. * indicates cell lines with a deleterious *BRCA1* or *BRCA2* mutation. **C**, To define HR status, cells were subjected to 10 Gy ionizing radiation, incubated for 6 h, fixed, co-stained for nuclear RAD51 and γH2AX, and imaged (100 cells/treatment). Scale bar = 5 μm **D**, Comparison of prexasertib $IC_{50}$ in cells with HRD ($n = 3$) versus HR proficiency ($n = 8$) using Wilcoxon rank sum test, $p = 0.918$. **E**, CHK1 expression by immunoblotting with cell lines on the left ordered by $IC_{50}$ to prexasertib and PEO1 cell line derivatives grouped to the right. **F**, Association between prexasertib $IC_{50}$ and CHK1 levels ($r = 0.686$). **G**, Whole cell lysates from indicated cell lines (ordered by $IC_{50}$ to prexasertib, with most sensitive on the left) were harvested for immunoblotting with β-actin (ACTB) as the loading control

cell lines or clones, including nine of HGSOC origin, to prexasertib, ceralasertib, and adavosertib (Fig. 3A) [26, 36, 37]. Mean prexasertib $IC_{50}$ values (Fig. 3B) ranged from 1.9 nM (CaOV3) to 12 nM (OVCAR5). Likewise, adavosertib and ceralasertib sensitivities varied across these cell lines (Fig. 3B).

Because of the established association between HR deficiency and sensitivity to platinum drugs as well as PARPis [4–6, 38–41], we assessed the relationship between RCM response and HR pathway integrity, as assessed by ionizing radiation (IR)-induced RAD51 foci, a standard assay to assess HR [42]. In contrast to the *BRCA2* mutant PEO1, which fail to form IR-induced RAD51 foci, the most sensitive (CaOV3) and least sensitive (COV362 and OVCAR5) lines readily formed IR-induced RAD51 foci as summarized in Fig. 3C, Fig. S3A and S3B. Moreover, the HR deficient HGSOC PEO1 line and HR proficient PEO4 line derived from the same patient later in the course of disease had similar $IC_{50}$s for each of the RCMs tested (Fig. 3A and B). Consistent with these observations, we failed to observe a significant relationship between HRD and RCM sensitivity across these ovarian cancer cell lines (Fig. 3D and S3C).

Across the cell lines, there was a weak correlation between prexasertib and adavosertib $IC_{50s}$ in the HR proficient lines (Fig. S3D) as has been reported in primary patient models of ovarian cancer [43]. In addition, there was a correlation between CHK1 levels and prexasertib $IC_{50}$ ($\rho = 0.69$, $p = 0.047$, Fig. 3E and F) as observed in the PDXs (Fig. S2G). In contrast, no significant association was observed between CHK1 levels and sensitivity to adavosertib or ceralasertib (Fig. S3E). Moreover, even though baseline levels of ATR and WEE1 also varied (Fig. 3G), they did not correlate with sensitivity to any of the three drugs.

#### Contribution of CDC25A to RCM-induced killing

Because HGSOC cells, which are usually *TP53* mutant or null, rely extensively on the intra-S and G2-M checkpoint regulators ATR, CHK1, and WEE1 to coordinate DNA repair and cell cycle progression [44], we assessed RCM-induced cell cycle changes in four HGSOC lines. After a 24-h prexasertib exposure, three of the lines arrested in S phase at concentrations below their $IC_{50}$ values from the clonogenics; and the fourth arrested in G2 (Fig. 4A and B). WEE1i treatment induced similar cell cycle effects, whereas ATRi treatment caused only a minor increase in the S phase population in the lines (Fig. S4A and B).

In further experiments, we examined key biological changes involved in S and G2 phase progression, focusing on the HGSOC cell lines PEO1 and COV362, which differ in genomic features and RCM sensitivity (Fig. 3B and S3B). In both lines, prexasertib induced a number of changes, including i) diminished CHK1 activity as manifested by reduced autophosphorylation at $Ser^{296}$; ii) decreased CHK1-mediated CDC25A phosphorylation, which led to increased CDC25A levels; and iii) and diminished CDK2 inhibitory phosphorylation, which resulted in increased CDK2 activity that was manifested by increased phosphorylation of the CDK2 substrate NPM1 on $Thr^{199}$ [23] as shown in Fig. 4C and D (lanes 2 and 3 vs. lane 1). Similar results were observed with the ATRi ceralasertib (Fig. 4C and D, lanes 6 and 7 vs. lane 1). The WEE1i adavosertib abolished CDK2 phosphorylation at $Tyr^{15}$, increased CDK2 activity, and increased RS, as manifested by increased γH2AX and phospho-RPA32, even though CHK1 activity (CHK1 $Ser^{296}$ autophosphorylation) was unaffected (Fig. 4C and D, lanes 4 and 5 vs. lane 1). Not surprisingly, the common feature of the three RCMs was enhancement of RS.

Examination of later effects after drug treatment indicated that a 5-day exposure to prexasertib (Fig. 4E and S4C), the oral CHK1i LY2880070 [45] (Fig. 4F), ceralasertib (Fig. S4D), or adavosertib (Fig. S4E) induced annexin V staining, a hallmark of apoptosis, at the same concentrations that induced cell cycle arrest at 24 h. Indeed, PEO1 and CaOV3 cells started to show signs of apoptosis even at concentrations below their $IC_{50}$s in colony forming assays. In contrast, the more resistant COV362 and OVCAR5 cells did not reach 50% cell death even at the highest concentrations, again demonstrating decreased drug response. In further experiments, CDC25 knockdown blunted this apoptosis, confirming the contribution of CDC25A upregulation to RCM-induced killing (Fig. 4G and S4F). Additional studies showed that procaspase 3 and PARP1, two well-established caspase substrates [46], were also cleaved, further supporting the view that cells were undergoing apoptosis after RCM treatment (Fig. 4H and I).

#### Contribution of JNK activation to cell death

To begin to assess the mechanism of this RCM-induced apoptosis, we performed RNAseq in CHK1i-treated PEO1 and COV362 cells. Despite a difference in the number of significantly altered ($|\log_2(FC)| > 1$, $p < 0.05$) transcripts, there was extensive overlap in the two lines (Fig. S5A). Multiple transcripts involved in cell death processes were upregulated (Fig. 5A), reflecting a stress gene signature (Fig. S5B) [47]. The upregulation of transcripts encoding components of the TNFα pathway (Fig. 5A purple labels and Fig. S5C), which has been implicated in RCM-induced apoptosis in monocytic leukemia cells [23], prompted us to examine the roles of JNK; the JNK substrate activator protein 1 (AP-1), a stress- and cytokine-activated transcription factor [48]; and the death receptor pathway in the HGSOC cells.

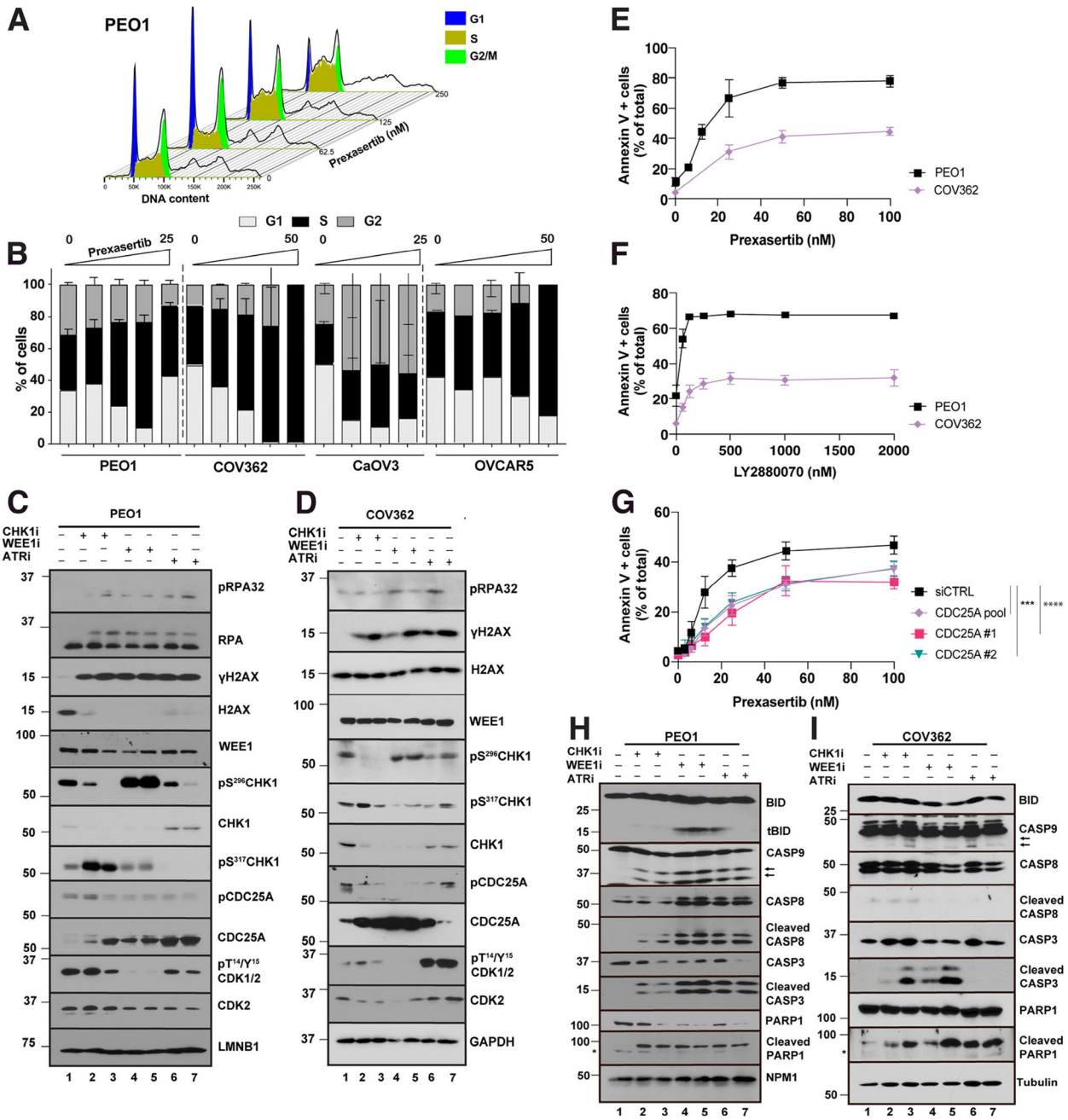


**Fig. 4** CDC25A contributes to CHK1i-induced apoptosis. **A**, Representative histogram showing cell cycle analysis in PEO1 cells treated with prexasertib for 24 h. **B**, Cell cycle distributions of PEO1, COV362, CaOV3, and Ovcar5 cells treated with increasing prexasertib for 24 h, stained with propidium iodide, and analyzed by flow cytometry. **C**, **D**, PEO1 (C) and COV362 (D) cells were treated with the caspase inhibitor Q-VD-OPh (5 μM) along with diluent, prexasertib (10 and 20 nM), ceralasertib (2 and 4 μM), or adavosertib (750 and 1000 nM) for 72 h and immunoblotted for indicated proteins. These concentrations were used in subsequent experiments unless otherwise specified. **E**, **F**, PEO1 and COV362 cells were treated with prexasertib (E) or LY2880070 (F) for 5 days and analyzed for Annexin V + cells by flow cytometry. **G**, Annexin V + cells in PEO1 cells treated with indicated siRNAs, followed by prexasertib treatment. siCDC25A pool vs siCTRL, ***$p < 0.001$; siCDC25A#1 vs siCTRL, ****$p < 0.0001$; siCDC25A#2 vs siCTRL, **$p < 0.001$ using two-way ANOVA with Dunnett's multiple comparisons test. **H**, **I**, PEO1 cells (H) and COV362 cells (I) were treated for 72 h with diluent, prexasertib, ceralasertib, or adavosertib in the absence of caspase inhibitors and analyzed for cleavage of caspase substrates. Error bars in B and E–G, mean ± SEM from 3 independent experiments. Arrows indicate cleavage products of caspase 9. * Indicates non-specific band

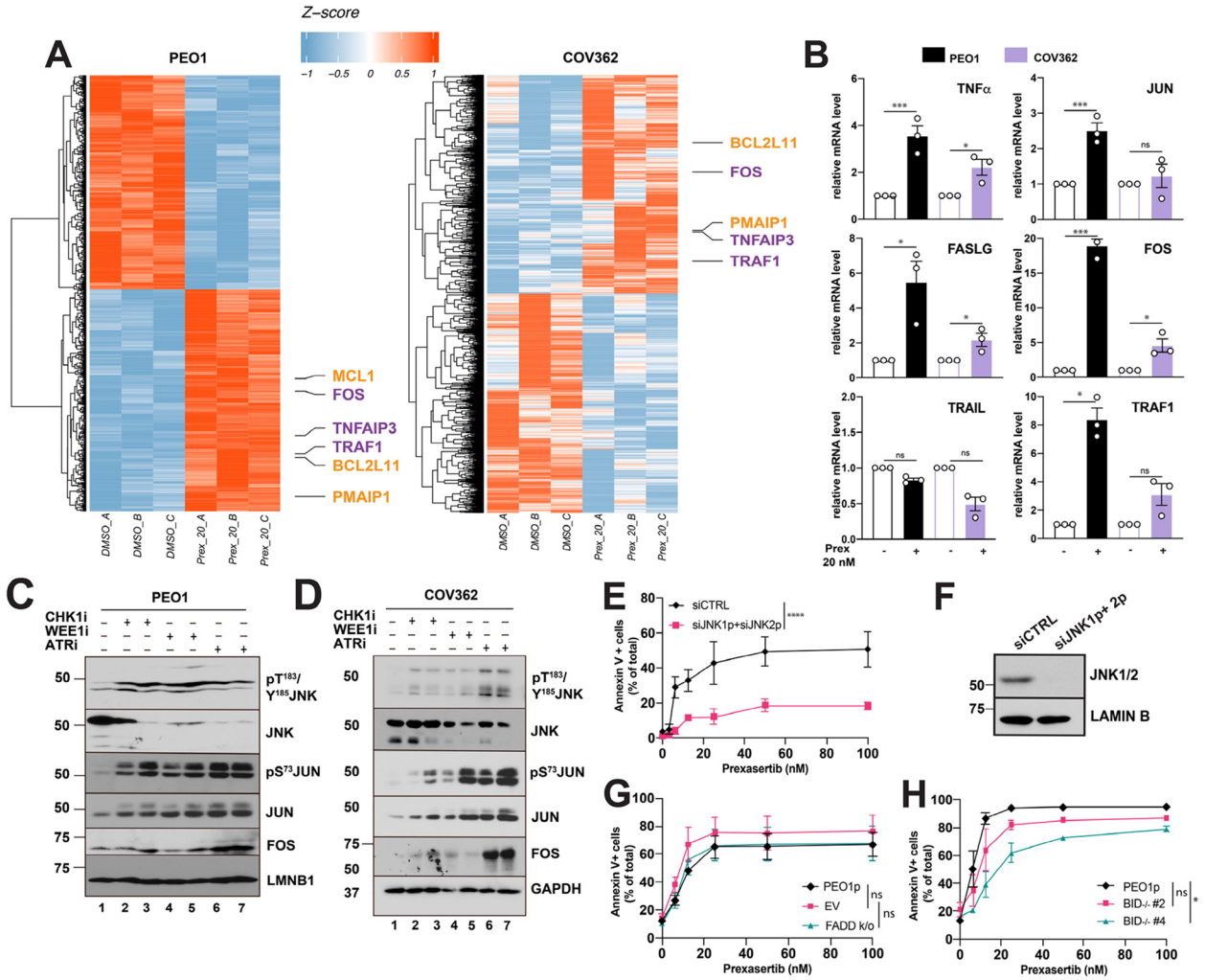


**Fig. 5** JNK and AP-1 stress responses promote CHK1i, ATRi and WEE1i apoptosis in ovarian carcinoma. **A**, Cells were treated with diluent or prexasertib (20 nM) for 48 h and analyzed by RNAseq. Biological replicates were prepared on three separate days. Heatmap comparing prexasertib treatment to vehicle in PEO1 (left) and COV362 (right). Differentially expressed apoptotic genes ($|log2FC| > 2$ and $p < 0.05$ by two-sided t-test, $n = 3$ per group) are noted in purple and orange. **B**, Aliquots of PEO1 and COV362 cells independent of those in panel A were treated for 48 h with prexasertib (20 nM) and assayed for the indicated mRNAs by qRT-PCR. **C**, **D**, PEO1 (C) and COV362 cells (D) treated with the caspase inhibitor Q-VD-OPh (5 μM) and diluent, prexasertib, ceralasertib, or adavosertib at the concentrations indicated for Fig. 4C were blotted for the indicated proteins. **E**, PEO1 cells were transfected with the indicated pools of siRNAs, treated with prexasertib for 5 days, and assayed for annexin V binding. **F**, Immunoblots to assess JNK levels in PEO1 cells transfected with the indicated siRNA pools. **G**, **H**, Pooled PEO1 cells transduced with empty vector (EV), FADD sgRNA (G) or BID sgRNA (H) were treated for 5 days with prexasertib and assayed for annexin binding. Error bars in B, E, G, and H, mean ± SEM of 3 independent experiments. *, *** and ****: $p < 0.05$, $p < 0.001$ and $p < 0.0001$, respectively, for indicated comparison by unpaired t-test corrected for multiple comparisons. *FADD*$^{-/-}$ vs PEO1 EV $p = 0.1585$; PEO1p vs PEO1 EV $p = 0.0786$; *BID*$^{-/-}$ #2 vs PEO1 EV $p = 0.1850$; *BID*$^{-/-}$ #4 vs PEO1 EV $p = 0.0286$ using two-way ANOVA with Dunnett's test for multiple comparisons

CHK1i-induced changes observed in the HGSOC lines included upregulation of the AP-1 components JUN and FOS, death ligands TNFα and FASLG (Fig. 5B-D), as well as upregulation of phospho-JUN and JUN, reflecting activation of the JNK pathway (Fig. 5C, D, and S5C). These changes were also observed in HGSOC cells treated with ceralasertib or adavosertib, suggesting a shared mechanism of cell death. Importantly, siRNA-mediated knockdown of JNK1 and JNK2 protected cells from CHK1i-induced apoptosis (Fig. 5E, F, and S5D-S5F). In contrast to AML, however, RCM-induced apoptosis in HGSOC cell lines was barely affected by CRISPR/Cas9-mediated knockout of *FADD* or *BID* (Fig. 5G, H, S5G and S5H), two proteins that play essential roles in death receptor-induced apoptosis (Fig. S5I, S5J and ref. 50). Collectively these observations suggest that JNK

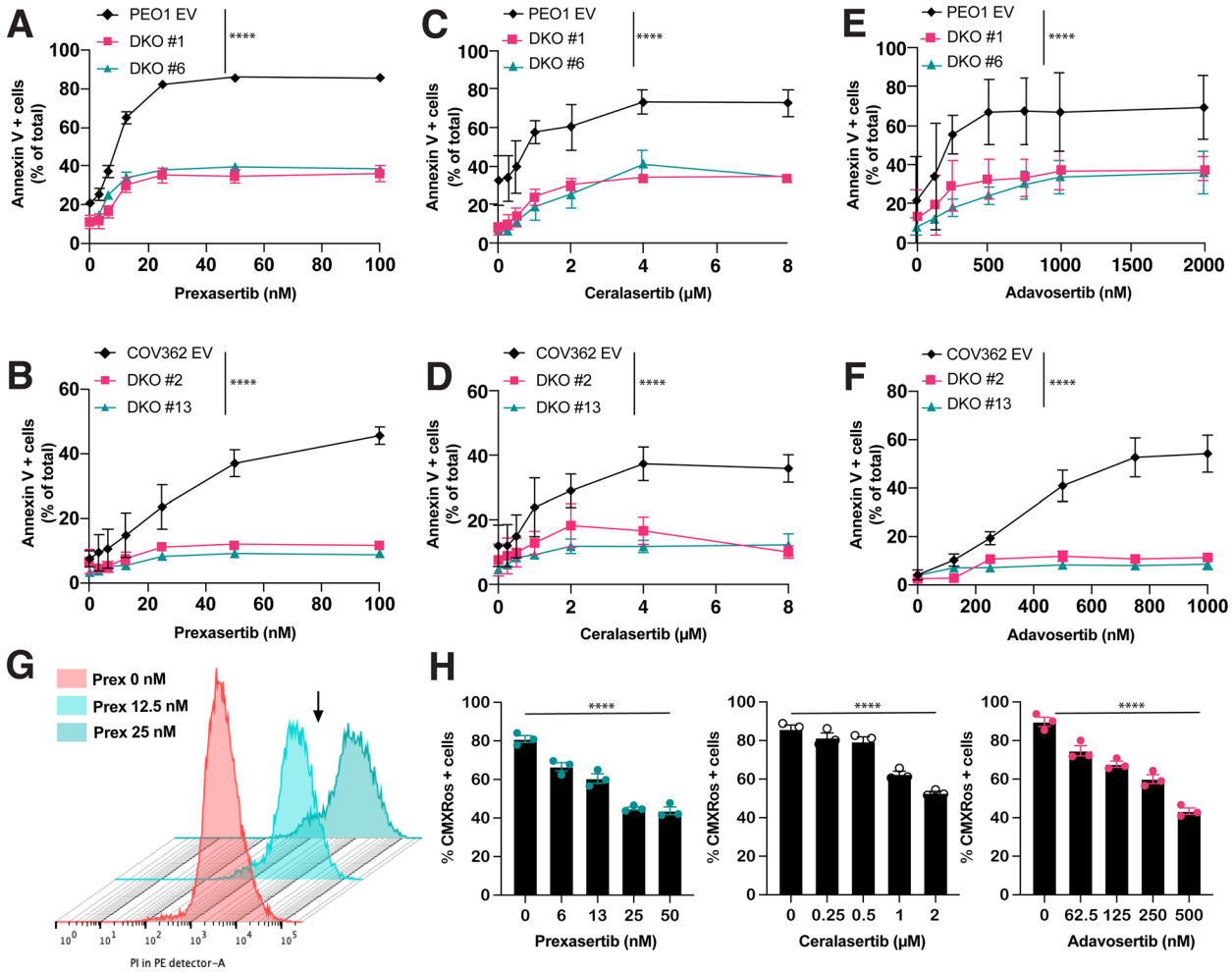


**Fig. 6** CHK1i, ATRi, and WEE1i-induced apoptosis is BAX- and BAK-dependent. **A-F**, Pooled PEO1 (A, C, E) or COV362 cells (B, D, F) transduced with empty vector (EV) or two separate *BAX/BAK* double knockout clones (DKO) were treated for 5 days with increasing prexasertib (A, B), ceralasertib (C, D), or adavosertib (E, F) and assayed for annexin binding. Error bars, mean ± SEM for 3 or more independent experiments. DKO#1, DKO#6 vs PEO1 EV ****$p < 0.0001$, DKO#2, DKO#13 vs COV362 EV ****$p < 0.0001$ using two-way ANOVA with Dunnett's test for multiple comparisons. **G**, Representative histogram showing CMXRos + cells treated with prexasertib for 5 days. Arrows indicate decrease in the fluorescence peak in prexasertib treated cells. **H**, Quantitation in PEO1 cells treated with increasing prexasertib, ceralasertib, or adavosertib concentrations for 5 days, stained with MitoTracker CMXRos, and analyzed by flow cytometry

signaling contributes to RCM-induced HGSOC cell death, but the upregulated death ligands do not.

### Contribution of BH3-only proteins BIM, BMF and PUMA

Because death receptor pathway interruption had limited impact on RCM-induced death of HGSOC cells, we next assessed the contribution of the mitochondrial apoptotic pathway. According to current understanding, activation of this pathway involves trafficking of BH3-only proteins to the mitochondrial surface, where they inhibit anti-apoptotic BCL2 family members and, under certain circumstances, directly activate the mitochondrial permeabilizers BAX and BAK [49, 50]. Loss of *BAX* and *BAK* (Fig. S6A and S6B) protected cells from cell death induced by prexasertib (Fig. 6A, B, and S6C) as well as ceralasertib and adavosertib (Fig. 6C-F). In addition, prexasertib, ceralasertib and adavosertib induced loss of mitochondrial outer membrane potential (Fig. 6G, H) as determined by CMXRos staining [51], confirming the occurrence of mitochondrial outer membrane permeabilization, a feature of the mitochondrial apoptotic pathway, during RCM-induced death.

Further inspection of the RNAseq data (Fig. 5A, orange labels) and subsequent qRT-PCR (Fig. 7A) revealed prominently upregulated transcripts encoding proteins in the mitochondrial apoptotic pathway, including the

BH3-only proteins NOXA, PUMA, and BIM. Consistent with these results, immunoblotting demonstrated increased NOXA as well as $BIM_L$ and $BIM_S$, lower molecular weight BIM splice variants that are more potent killers [52], in RCM-treated HGSOC cell lines, although PUMA was not consistently upregulated at the protein level (Fig. 7B and C, lanes 2–7 vs lane 1). Moreover, mitochondrial fractions from COV362 and PEO1 cells were found to contain more $BIM_L$ and BMF after prexasertib treatment (Fig. 7D, E), suggesting their release from sites of sequestration and translocation to the mitochondria [49, 50], events previously reported to occur downstream of JNK activation in cells undergoing anoikis [24, 25]. In addition, NOXA was increased in the COV362 mitochondria.

To assess the contribution of these changes to RCM-induced killing, BH3-only proteins were knocked down individually and in combinations. Depletion of the individual BH3-only proteins BIM, BMF, PUMA, or NOXA offered limited protection (Fig. S7A and S7B). In contrast, combined knockdown of PUMA + BMF or PUMA + BIM decreased prexasertib-induced apoptosis by > 40%, and knockdown of PUMA + BMF + BIM (siPBB) almost completely protected cells (Fig. 7F and G). Knockdown of additional BH3-only proteins, including BID and NOXA (siPBBBN), diminished apoptosis to the same extent as siPBB, suggesting that BMF, BIM, and PUMA are the critical BH3-only proteins in this process.

Collectively, these results establish a molecular framework linking RCM treatment to mitochondrial apoptosis in which CHK, ATR, or WEE1 inhibition leads to stabilization of CDC25A, S phase dysfunction, sustained JNK signaling, and activation of the BH3-only proteins PUMA, BIM, and BMF, leading to BAX/BAK-mediated apoptosis (Fig. 7H). With this framework in hand, we examined PDX samples harvested on day 8 of therapy during the HGSOC PDX study shown in Fig. 2. While it is not possible to assess changes in BH3-only protein expression in vivo because cells with the greatest BH3-only protein increase undergo apoptosis and are lost from the analysis in the absence of caspase inhibitors [53], examination of upstream mediators of this pathway (Fig. 7I) indicated that adavosertib induced complete CDK2 dephosphorylation, increased CDK2 activity and increased JNK phosphorylation in the models that showed objective tumor shrinkage (PH354 and PH061, lanes 4–6 vs lanes 1–3) but not in models that failed to shrink (PH235 and PH063). In accordance with the significant tumor slowing induced by ceralasertib in PH354 and PH061, the tumors harvested on Day 8 after ATRi also displayed reduced CDK2 activity and increased JNK phosphorylation (Fig. 7I, lanes 7–9 vs lanes 1–3, models PH354 and PH061), suggesting that levels of activated CDK2 and JNK in HGSOC tumors might be useful pharmacodynamic biomarkers that predict subsequent response to RCM therapy.

## Discussion

The RCMs studied here, inhibitors of CHK1, ATR, and WEE1, have shown tantalizing but inconsistent clinical activity against HGSOC, suggesting the need for better understanding of their action to identify neoplasms most likely to respond. To facilitate the clinical development of these classes of agents, the present study has systematically examined the pathway of cytotoxic signaling that starts with the inhibition of replication checkpoint kinases and culminates in the activation of the mitochondrial apoptotic pathway in HGSOC cells (Fig. 7H).

One of the goals in studying RCM activity in model systems is to identify biomarkers that predict response. Even though an increasing number of clinical trials are interrogating expression of CCNE1 and MYC as determinants of RCM response [22, 54], our examination of multiple PDXs treated with RCMs in vivo or ex vivo indicated that HGSOC responses to RCMs appear to be independent of CCNE1 or MYC expression (Figs. 1, 2, and S2). Instead,

(See figure on next page.)

**Fig. 7** CHK1i, ATRi, and WEE1i-induced apoptosis in ovarian cancer cells is driven by combined action of PUMA, BIM and BMF. **A**, PEO1 and COV362 cells were treated for 48 h with prexasertib (20 nM) and assayed for the indicated mRNA by qRT-PCR. Error bars, ± SEM of 3 independent experiments. *, ** and ***, $p < 0.05$, $p < 0.01$, and $p < 0.001$ respectively, for indicated comparison by unpaired t-test corrected for multiple comparisons. **B**, **C**, PEO1 (B) and COV362 cells (C) were treated with the caspase inhibitor Q-VD-OPh (5 μM) and diluent, prexasertib, ceralasertib, or adavosertib as indicated for Fig. 4C for 72 h and immunoblotted for the indicated BH3 proteins. **D**, **E**, After PEO1 (D) and COV362 (E) cells treated with prexasertib (20 nM) + the caspase inhibitor Q-VD-OPh (5 μM) for 72 h, whole cell lysates, cytosol, and mitochondria were isolated and probed for the indicated proteins. GSTπ and MCL1 served as markers of the cytosolic and mitochondrial fractions respectively. **F**, 24 h after PEO1 cells were transfected with the indicated siRNAs, prexasertib (20 nM) was added for 5 days and cells were assayed for AnnexinV binding. Error bars, mean ± SEM from 3 or more independent experiments. siPUMA-BIM and siPUMA-BMF vs siCTRL, $p < 0.01$; siPUMA-BIM-BMF-BID-NOXA (siPBBBN) vs siCTRL, $p < 0.001$; siPUMA-BIM-BMF (siPBB) vs siCTRL, $p < 0.0001$ using two-way ANOVA with Dunnett's test for multiple comparisons. **G**, Immunoblots to assess BH3-only protein levels in PEO1 cells transfected with the indicated siRNA combinations. **H**, Schematic of BH3-only protein-mediated apoptosis induced by RCMs. **I**, Immunoblot analysis of potential response predictors in the two $CCNE^{amp}MYC^{amp}$ PDXs PH354 and PH235 (top, blue) in comparison to WT PDXs PH061 and PH063 (bottom, black). Each lane contains tumor from a single PDX-bearing mouse after 8 days of the indicated treatments. Dashed line indicates removal of lanes from mice on a separate study

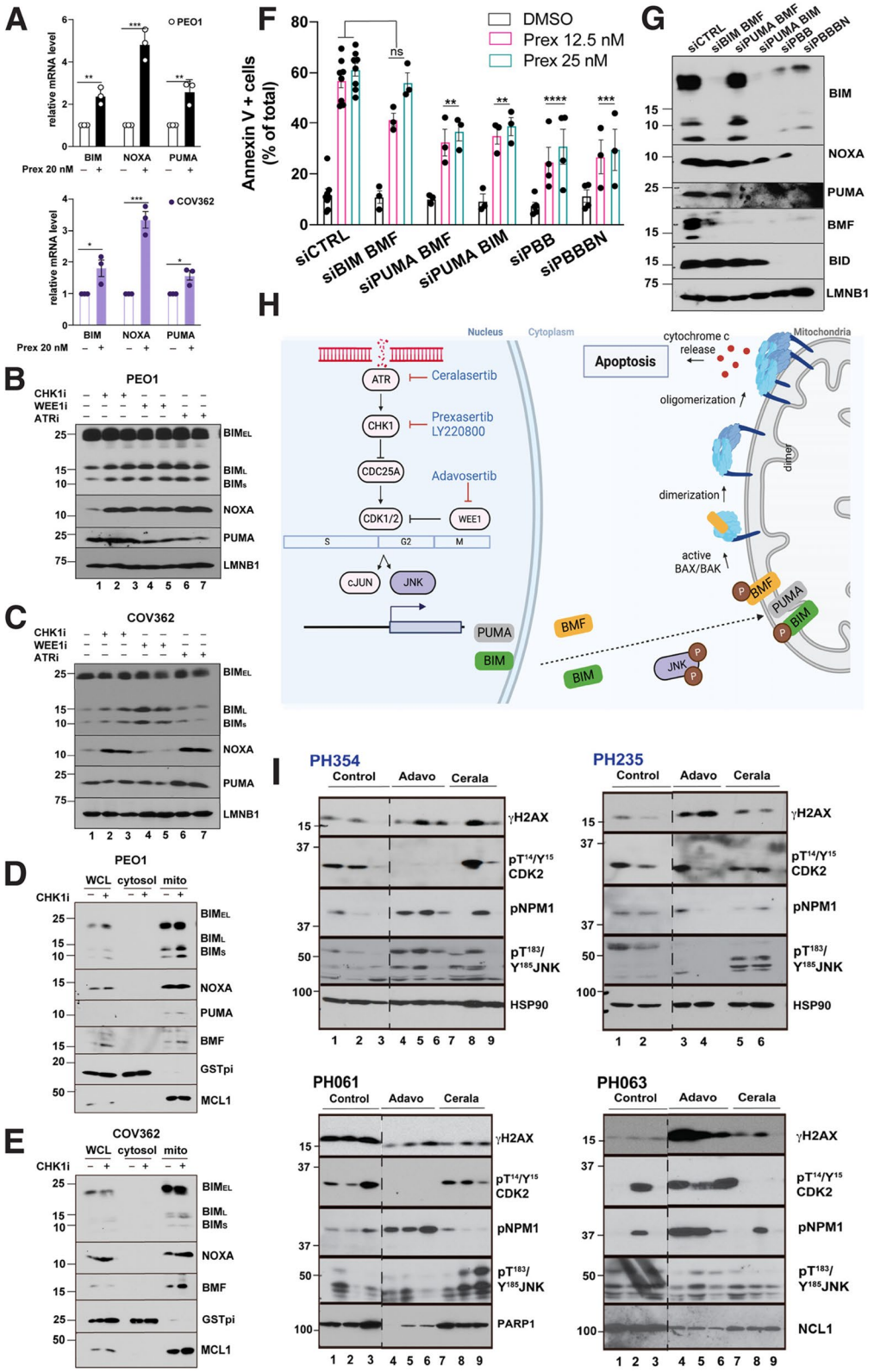


**Fig. 7** (See legend on previous page.)

the present study found that prexasertib responses are associated with low CHK1 protein levels (Fig. 3 and S2), in agreement with results in lung cancers and acute leukemias [23, 55]. Thus, CHK1 levels might need to be evaluated in further studies right along with the recently proposed predictive biomarkers BLM, a helicase involved in ATR-mediated fork stabilization after stress, and the WEE1 regulator FAM112A [56, 57].

In addition to predictive markers, there is great interest in improved pharmacodynamic biomarkers of RCM activity. The present study implicates CDC25A as a potentially important contributor to CHK1i anti-cancer effects that is upregulated during CHK1i and WEE1i therapy (Fig. 4). Moreover, examination of the transcriptomic and signaling changes during RCM treatment identified a series of transcripts, constituting part of a stress gene signature [47], that were upregulated in both of the HGSOC cell lines characterized by RNAseq after drug treatment (Fig. 5 and S5). Consistent with these results, we observed that RCMs activated the JNK pathway, which plays a critical role in RCM-induced cytotoxicity as indicated by the effects of JNK knockdown (*op cit.*). Further analysis indicated that mRNAs encoding a number of death ligands, including TNFα and FASL, were upregulated by RCM treatment. Notably, however, interruption of the extrinsic apoptotic pathway afforded HGSOC cells little protection from RCM-induced cell death (Fig. 5). This lack of involvement of death ligands in RCM-induced killing of HGSOC cells is in contrast to the role of JUN-mediated *TNF* transactivation in RCM-induced killing of acute monocytic leukemia cells [23], illustrating variation in cytotoxic pathways activated by RCMs in different cell types. Instead, RCM-induced cell death in HGSOC cells depends on the mitochondrial apoptotic pathway, as indicated by the loss of mitochondrial membrane potential (Fig. 6H), which reflects mitochondrial permeabilization, as well as the protective effects of knocking out *BAX* and *BAK* (Fig. 6A-F) or knocking down the BH3-only proteins BIM, BMF, and PUMA (Fig. 7F and S7), three established initiators of the mitochondrial pathway [49, 58] that traffic to mitochondria during RCM treatment (Fig. 7D and E). Importantly, involvement of BMF, a BH3-only protein previously implicated mainly in anoikis, also illustrates a way in which the downstream portion of the RCM cytotoxicity pathway is also potentially unique compared to other antineoplastic agents. Indeed, the present observations identify critical steps distal to effects at replication forks that must occur for RCMs to be cytotoxic, suggest additional signaling events that can be interrogated to determine whether components of the replication checkpoint have been successfully inhibited, and imply that factors capable of inhibiting the mitochondrial pathway, e.g., amplifications of the loci encoding BCLXL or MCL1 that are commonly observed in ovarian cancer, might need to be considered in identifying patients for treatment with RCMs.

Analysis of the HGSOC PDXs treated in vivo indicated that H2AX phosphorylation was detectable at baseline and increased with RCM treatment in three of four PDXs, including two PDXs that did not show regressions (Fig. 7). In contrast, CDK2 phosphorylation was completely inhibited only in the two PDXs that shrank during adavosertib treatment and not in the two that failed to shrink (Fig. 7I), establishing inhibition of CDK2 phosphorylation as a potentially important pharmacodynamic indicator of adavosertib action as well. More broadly, the present analysis identified upregulation of CDC25A, dephosphorylation and activation of CDK2, and activation of JNK1/2 as evaluable steps that might be productively interrogated in future RCM clinical trials.

While the present studies utilized prexasertib, adavosertib and ceralasertib, it is important to recognize that these are well-established inhibitors that can be viewed as paradigm drugs. Prexasertib, which has exhibited promising activity in HR proficient ovarian cancer [23], remains in clinical trials as ACR-368 (Clinical Trials.gov identifier NCT05548296). Although adavosertib and ceralasertib are being supplanted by orally bioavailable agents for further testing as monotherapies and in combinations, it is anticipated that the newer agents will induce the same signaling described here.

In summary, the present results provide new mechanistic insight into therapies targeting the DNA damage response and provide preclinical data to support a series of potential biomarkers for further testing as RCMs undergo additional clinical development.

## Conclusions

While numerous studies over the past decade have contributed to current understanding of how replication checkpoint modulators impact cell cycle regulation, there is limited understanding of how the resulting changes ultimately kill susceptible cells. Recent trials indicate the clinical benefit of prexasertib monotherapy in the setting of platinum-resistant *CCNE*$^{amp}$ cancer, the response is still heterogeneous, and outcomes are dismal. Our findings suggest a model in which replication stress results in the activation of JNK and AP-1 to effect two sets of distinct changes, i) upregulation of PUMA and BIM mRNAs and ii) displacement of BIM and BMF from sites of sequestration so they can directly and/or indirectly activate BAX/BAK at the mitochondrial outer membrane. Measurement of all of these steps and perhaps more will be required to understand the which ovarian cancer patients will benefit from these therapies.

**Abbreviations**

| | |
|---|---|
| AML | Acute myelogenous leukemia |
| AP-1 | Activator protein 1 |
| ATR | Ataxia-telangiectasia-mutated-and-Rad3-related |
| ATRi | Ataxia-telangiectasia-mutated-and-Rad3-related kinase inhibitor |
| CDK | Cyclin dependent kinase |
| CHK1 | Checkpoint kinase 1 |
| CHK1i | Checkpoint kinase 1 inhibitor |
| DDR | DNA damage response |
| HGSOC | High grade serous ovarian cancer |
| HR | Homologous recombination |
| HRD | Homologous recombination deficiency |
| JNK | C-JUN N-terminal kinases |
| OC | Ovarian cancer |
| p53 | Tumor protein p53 |
| PARP | Poly(ADP-ribose) polymerase |
| PARPi | Poly(ADP-ribose) polymerase inhibitor |
| PDX | Patient-derived xenograft |
| RCM | Replication checkpoint modulators |
| RS | Replication stress |

## Supplementary Information

The online version contains supplementary material available at https://doi.org/10.1186/s12943-024-02125-5.

Supplementary Material 1.

Supplementary Material 2.

**Acknowledgements**
We thank David Toft and Guy Poirier for kind gifts of antibodies as well as investigators at Astra-Zeneca for providing adavosertib and ceralasertib for PDX studies.

**Disclosure of potential conflicts of interest**
No potential conflicts of interest were disclosed.

**Authors' contributions**
A.V. contributed to the conception of the project, performed and analyzed experiments, prepared figures, and wrote the manuscript; C.C. performed the bioinformatic analysis, contributed to results interpretation, and manuscript preparation; K.L.P., X.H., P.A.S., A.R.S., K.S.F., C.C.S., and L.N.D. performed experiments, analyzed data, and helped prepare figures for the manuscript; E.A.B. and C.D.M. contributed to the interpretation of results; M.C.L performed statistical analysis and prepared figures for the manuscript; X.W.M. generated CRISPR lines; N.D.V and H.D. contributed to manuscript preparation; A.L.O provided statistical expertise, analysed data and contributed to manuscript preparation; F.J.C., and E.M.S. contributed to the characterization of PDX models; H.L. provided computational expertise; S.J.W. contributed to planning of animal studies, interpretation of data and preparation of manuscript; S.H.K. conceived the project, wrote grants, planned experiments, interpreted data, and wrote the manuscript. All authors contributed to the writing/or critical review of the manuscript.

**Funding**
This work was supported in part by grants from the National Cancer Institute (R01 CA172503 to S.H.K.; P50 CA136393 to S.H.K., A.L.O. and S.J.W.; F30 CA213737 to C.D.M.; R35 CA253187 to F.J.C.; and R01 CA225662 to F.J.C. and S.J.W.) as well as a grant from the Ovarian Cancer Research Alliance (S.H.K. and E.M.S.) and Stand Up to Cancer SU2C-AACR-DT16-15 (E.M.S. and S.H.K.).

**Availability of data and materials**
The RNA-seq datasets discussed in this publication are accessible through GEO series accession number GSE215340.

## Declarations

**Ethics approval and consent to participate**
All procedures were conducted in accordance with Animal Welfare Regulations and were approved by the Institutional Animal Care and Use Committee (IACUC) at the Mayo Clinic (A37615).

**Competing interests**
The authors declare no competing interests.

Received: 23 May 2024 Accepted: 17 September 2024
Published online: 07 October 2024

**References**

1. Siegel RL, Miller KD, Wagle NS, Jemal A. Cancer statistics, 2023. CA Cancer J Clin. 2023;73:17–48.
2. Geistlinger L, Oh S, Ramos M, Schiffer L, LaRue RS, Henzler CM, et al. Multiomic analysis of subtype evolution and heterogeneity in high-grade serous ovarian carcinoma. Cancer Res. 2020;80:4335–45.
3. Sung H, Ferlay J, Siegel RL, Laversanne M, Soerjomataram I, Jemal A, et al. Global cancer statistics 2020: GLOBOCAN estimates of incidence and mortality worldwide for 36 cancers in 185 countries. CA Cancer J Clin. 2021;71:209–49.
4. Konstantinopoulos PA, Ceccaldi R, Shapiro GI, D'Andrea AD. Homologous recombination deficiency: exploiting the fundamental vulnerability of ovarian cancer. Cancer Discov. 2015;5:1137–54.
5. Coleman RL, Oza AM, Lorusso D, Aghajanian C, Oaknin A, Dean A, et al. Rucaparib maintenance treatment for recurrent ovarian carcinoma after response to platinum therapy (ARIEL3): a randomised, double-blind, placebo-controlled, phase 3 trial. Lancet. 2017;390:1949–61.
6. Moore K, Colombo N, Scambia G, Kim BG, Oaknin A, Friedlander M, et al. Maintenance olaparib in patients with newly diagnosed advanced ovarian cancer. N Engl J Med. 2018;379:2495–505.
7. Gonzalez-Martin A, Pothuri B, Vergote I, DePont CR, Graybill W, Mirza MR, et al. Niraparib in patients with newly diagnosed advanced ovarian cancer. N Engl J Med. 2019;381:2391–402.
8. DiSilvestro P, Banerjee S, Colombo N, Scambia G, Kim BG, Oaknin A, et al. Overall Survival With Maintenance Olaparib at a 7-Year Follow-Up in Patients With Newly Diagnosed Advanced Ovarian Cancer and a BRCA Mutation: The SOLO1/GOG 3004 Trial. J Clin Oncol. 2023;41:609–17.
9. Bowry A, Kelly RDW, Petermann E. Hypertranscription and replication stress in cancer. Trends Cancer. 2021;7:863–77.
10. McDermott JE, Arshad OA, Petyuk VA, Fu Y, Gritsenko MA, Clauss TR, et al. Proteogenomic characterization of ovarian hgsc implicates mitotic kinases, replication stress in observed chromosomal instability. Cell Rep Med. 2020;1:1.
11. Huntoon CJ, Flatten KS, Wahner Hendrickson AE, Huehls AM, Sutor SL, Kaufmann SH, et al. ATR Inhibition Broadly Sensitizes Ovarian Cancer Cells to Chemotherapy Independent of BRCA Status. Cancer Res. 2013;73:3683–91.
12. da Costa A, Chowdhury D, Shapiro GI, D'Andrea AD, Konstantinopoulos PA. Targeting replication stress in cancer therapy. Nat Rev Drug Discov. 2023;22:38–58.
13. Konstantinopoulos PA, da Costa A, Gulhan D, Lee EK, Cheng SC, Hendrickson AEW, et al. A Replication stress biomarker is associated with response to gemcitabine versus combined gemcitabine and ATR inhibitor therapy in ovarian cancer. Nat Commun. 2021;12:5574.
14. Lheureux S, Cristea MC, Bruce JP, Garg S, Cabanero M, Mantia-Smaldone G, et al. Adavosertib plus gemcitabine for platinum-resistant or platinum-refractory recurrent ovarian cancer: a double-blind, randomised, placebo-controlled, phase 2 trial. Lancet. 2021;397:281–92.
15. Miller WH, Shields AF, Provencher D, Gilbert L, Shapiro G, Oza AM, et al. A phase I/II study of oral chk1 inhibitor LY2880070 in combination with low-dose gemcitabine in patients with advanced or metastatic ovarian cancer. Ann Oncol. 2022;33:S793–4.

16. Moore KN, Hong DS, Patel MR, Pant S, Ulahannan SV, Jones S, et al. A phase 1b trial of prexasertib in combination with standard-of-care agents in advanced or metastatic cancer. Target Oncol. 2021;16:569–89.
17. Do K, Wilsker D, Ji J, Zlott J, Freshwater T, Kinders RJ, et al. Phase I study of single-agent AZD1775 (MK-1775), a Wee1 kinase inhibitor, in patients with refractory solid tumors. J Clin Oncol. 2015;33:3409–15.
18. Lee JM, Nair J, Zimmer A, Lipkowitz S, Annunziata CM, Merino MJ, et al. Prexasertib, a cell cycle checkpoint kinase 1 and 2 inhibitor, in BRCA wild-type recurrent high-grade serous ovarian cancer: a first-in-class proof-of-concept phase 2 study. Lancet Oncol. 2018;19(2):207–15.
19. Konstantinopoulos PA, Lee JM, Gao B, Miller R, Lee JY, Colombo N, et al. A Phase 2 study of prexasertib (LY2606368) in platinum resistant or refractory recurrent ovarian cancer. Gynecol Oncol. 2022;167(2):213–25.
20. Yap TA, O'Carrigan B, Penney MS, Lim JS, Brown JS, de Miguel Luken MJ, et al. Phase I trial of first-in-class ATR inhibitor M6620 (VX-970) as monotherapy or in combination with carboplatin in patients with advanced solid tumors. J Clin Oncol. 2020;38:3195–204.
21. Giudice E, Huang TT, Nair JR, Zurcher G, McCoy A, Nousome D, et al. The CHK1 inhibitor prexasertib in BRCA wild-type platinum-resistant recurrent high-grade serous ovarian carcinoma: a phase 2 trial. Nat Commun. 2024;15:2805.
22. Au-Yeung G, Bressel M, Prall O, Surace D, Andrews J, Mongta S, et al. IGNITE: A phase II signal-seeking trial of adavosertib targeting recurrent high-grade, serous ovarian cancer with cyclin E1 overexpression with and without gene amplification. J Clin Oncol. 2022;40: 5515.
23. Ding H, Vincelette ND, McGehee CD, Kohorst MA, Koh BD, Venkatachalam A, et al. CDK2-Mediated Upregulation of TNFalpha as a mechanism of selective cytotoxicity in acute leukemia. Cancer Res. 2021;81:2666–78.
24. Lei K, Davis RJ. JNK phosphorylation of Bim-related members of the Bcl2 family induces Bax-dependent apoptosis. Proc Natl Acad Sci U S A. 2003;100:2432–7.
25. Girnius N, Davis RJ. JNK Promotes epithelial cell anoikis by transcriptional and post-translational regulation of BH3-only proteins. Cell Rep. 2017;21:1910–21.
26. Domcke S, Sinha R, Levine DA, Sander C, Schultz N. Evaluating cell lines as tumour models by comparison of genomic profiles. Nat Commun. 2013;4:2126.
27. Sakai W, Swisher EM, Jacquemont C, Chandramohan KV, Couch FJ, Langdon SP, et al. Functional restoration of BRCA2 protein by secondary BRCA2 mutations in BRCA2-mutated ovarian carcinoma. Cancer Res. 2009;69:6381–6.
28. Al Hilli MM, Becker MA, Weroha SJ, Flatten KS, Hurley RM, Harrell MI, et al. In vivo anti-tumor activity of the PARP inhibitor niraparib in homologous recombination deficient and proficient ovarian carcinoma. Gynecol Oncol. 2016;143:379–88.
29. Weroha SJ, Becker MA, Enderica-Gonzalez S, Harrington SC, Oberg AL, Maurer MJ, et al. Tumorgrafts as in vivo surrogates for women with ovarian cancer. Clin Cancer Res. 2014;20:1288–97.
30. Abeykoon JP, Wu X, Nowakowski KE, Dasari S, Paludo J, Weroha SJ, et al. Salicylates enhance CRM1 inhibitor antitumor activity by induction of S-phase arrest and impairment of DNA-damage repair. Blood. 2021;137:513–23.
31. Li M, Balch C, Montgomery JS, Jeong M, Chung JH, Yan P, et al. Integrated analysis of DNA methylation and gene expression reveals specific signaling pathways associated with platinum resistance in ovarian cancer. BMC Med Genomics. 2009;2: 34.
32. Etemadmoghadam D, deFazio A, Beroukhim R, Mermel C, George J, Getz G, et al. Integrated genome-wide DNA copy number and expression analysis identifies distinct mechanisms of primary chemoresistance in ovarian carcinomas. Clin Cancer Res. 2009;15:1417–27.
33. Murga M, Campaner S, Lopez-Contreras AJ, Toledo LI, Soria R, Montana MF, et al. Exploiting oncogene-induced replicative stress for the selective killing of Myc-driven tumors. Nat Struct Mol Biol. 2011;18:1331–5.
34. Goehring L, Huang TT. WEE1i-ATRi combination therapy: a promising low-dose treatment for CCNE1-amplified gynecologic cancers. Cell Rep Med. 2021;2: 100402.
35. Xu H, George E, Kinose Y, Kim H, Shah JB, Peake JD, et al. CCNE1 copy number is a biomarker for response to combination WEE1-ATR inhibition in ovarian and endometrial cancer models. Cell Rep Med. 2021;2: 100394.
36. Coscia F, Watters KM, Curtis M, Eckert MA, Chiang CY, Tyanova S, et al. Integrative proteomic profiling of ovarian cancer cell lines reveals precursor cell associated proteins and functional status. Nat Commun. 2016;7:12645.
37. Zhang H, Liu T, Zhang Z, Payne SH, Zhang B, McDermott JE, et al. Integrated proteogenomic characterization of human high-grade serous ovarian cancer. Cell. 2016;166:755–65.
38. Cass I, Baldwin RL, Varkey T, Moslehi R, Narod SA, Karlan BY. Improved survival in women with BRCA-associated ovarian carcinoma. Cancer. 2003;97:2187–95.
39. Pennington KP, Walsh T, Harrell MI, Lee MK, Pennil CC, Rendi MH, et al. Germline and somatic mutations in homologous recombination genes predict platinum response and survival in ovarian, fallopian tube, and peritoneal carcinomas. Clin Cancer Res. 2014;20:764–75.
40. Lord CJ, Ashworth A. Mechanisms of resistance to therapies targeting BRCA-mutant cancers. Nat Med. 2013;19:1381–8.
41. O'Connor MJ. Targeting the DNA damage response in cancer. Mol Cell. 2015;60:547–60.
42. Tashiro S, Walter J, Shinohara A, Kamada N, Cremer T. Rad51 accumulation at sites of DNA damage and in postreplicative chromatin. J Cell Biol. 2000;150:283–91.
43. Golder A, Nelson L, Tighe A, Barnes B, Coulson-Gilmer C, Morgan RD, et al. Multiple-low-dose therapy: effective killing of high-grade serous ovarian cancer cells with ATR and CHK1 inhibitors. NAR. Cancer. 2022;4:zcac036.
44. Saldivar JC, Hamperl S, Bocek MJ, Chung M, Bass TE, Cisneros-Soberanis F, et al. An intrinsic S/G2 checkpoint enforced by ATR. Science. 2018;361:806–10.
45. Huffman BM, Feng H, Parmar K, Wang J, Kapner KS, Kochupurakkal B, et al. A phase I expansion cohort study evaluating the safety and efficacy of the CHK1 nhibitor LY2880070 with low-dose gemcitabine in patients with metastatic pancreatic adenocarcinoma. Clin Cancer Res. 2023;29:5047–56.
46. Earnshaw WC, Martins LM, Kaufmann SH. Mammalian caspases: structure, activation, substrates and functions during apoptosis. Annu Rev Biochem. 1999;68:383–424.
47. Zhang K, Erkan EP, Jamalzadeh S, Dai J, Andersson N, Kaipio K, et al. Longitudinal single-cell RNA-seq analysis reveals stress-promoted chemoresistance in metastatic ovarian cancer. Sci Adv. 2022;8: eabm1831.
48. Eferl R, Wagner EF. AP-1: a double-edged sword in tumorigenesis. Nat Rev Cancer. 2003;3:859–68.
49. Taylor RC, Cullen SP, Martin SJ. Apoptosis: controlled demolition at the cellular level. Nat Rev Mol Cell Biol. 2008;9:231–41.
50. Walensky LD. Targeting BAX to drug death directly. Nat Chem Biol. 2019;15:657–65.
51. Pan R, Ryan J, Pan D, Wucherpfennig KW, Letai A. Augmenting NK cell-based immunotherapy by targeting mitochondrial apoptosis. Cell. 2022;185(1521–38): e18.
52. Puthalakath H, Huang DCS, O'Reilly LA, King SM, Strasser A. The proapoptotic activity of the Bcl-2 family member bim is regulated by interaction with the dynein motor complex. Mol Cell. 1999;3:287–96.
53. Yun S, Vincelette ND, Knorr KL, Almada LL, Schneider PA, Peterson KL, et al. 4EBP1/c-MYC/PUMA and NF-kappaB/EGR1/BIM pathways underlie cytotoxicity of mTOR dual inhibitors in malignant lymphoid cells. Blood. 2016;127:2711–22.
54. Fu S, Yao S, Yuan Y, Previs RA, Elias AD, Carvajal RD, et al. Multicenter phase II trial of the WEE1 Inhibitor adavosertib in refractory solid tumors harboring CCNE1 Amplification. J Clin Oncol. 2023;41:1725–34.
55. Sen T, Tong P, Stewart CA, Cristea S, Valliani A, Shames DS, et al. CHK1 Inhibition in Small-Cell lung cancer produces single-agent activity in biomarker-defined disease subsets and combination activity with cisplatin or olaparib. Cancer Res. 2017;77:3870–84.
56. Gupta N, Huang TT, Nair JR, An D, Zurcher G, Lampert EJ, et al. BLM overexpression as a predictive biomarker for CHK1 inhibitor response in PARP inhibitor-resistant BRCA-mutant ovarian cancer. Sci Transl Med. 2023;15: eadd7872.

57. Li F, Kozono D, Deraska P, Branigan T, Dunn C, Zheng XF, et al. CHK1 inhibitor blocks phosphorylation of FAM122A and promotes replication stress. Mol Cell. 2020;80(410–22): e6.
58. Strasser A, Cory S, Adams JM. Deciphering the rules of programmed cell death to improve therapy of cancer and other diseases. EMBO J. 2011;30:3667–83.

## Publisher's Note